Supporting Information for

**An ARGO and XBT observing system for the Atlantic Meridional Overturning Circulation and Meridional Heat Transport (AXMOC) at 22.5ºS**

**I. Pita[1,2,3], M. Goes[2,3], D. L. Volkov[2,3], S. Dong[3], G. Goni[3] and M. Cirano[4]**

[1]Rosenstiel School, University of Miami, Miami, Fl, United States of America.

[2]Cooperative Institute for Marine and Atmospheric Studies, University of Miami, Miami, Fl, United States of America.

[3]Atlantic Ocean and Metrorological Laboratory, NOAA, United States of America.

[4]Department of Meteorology, Institude of Geosciences, Federal university of Rio de Janeiro (UDRJ), Brazil

Corresponding author: Ivenis Pita ([ivenis.pita@noaa.gov](mailto:ivenis.pita@noaa.gov))

**Contents of this file**

> Text S1 to S4
> Figures S1 to S4

**Introduction**

The supplementary material could be divided in 2 parts. The figure S1 is an extension of Figure 8 analysis, where WOCE data is compared to AXMOC data for a similar period, and the Figures S2-S4 compares the AMOC and MHT at 22.5°S between AXMOC and other databases (synthetic estimations and model reanalysis).

**Text S1.**

Figure S1 is an extension of the Figure 8 analysis. Here, WOCE temperature, salinity, dissolved oxygen and meridional velocity sections at 24°S are compared to temperature, salinity and meridional velocity sections at 22.5°S for March 2018. Figure S1 corroborates with the conclusions drawn from Figure 8.
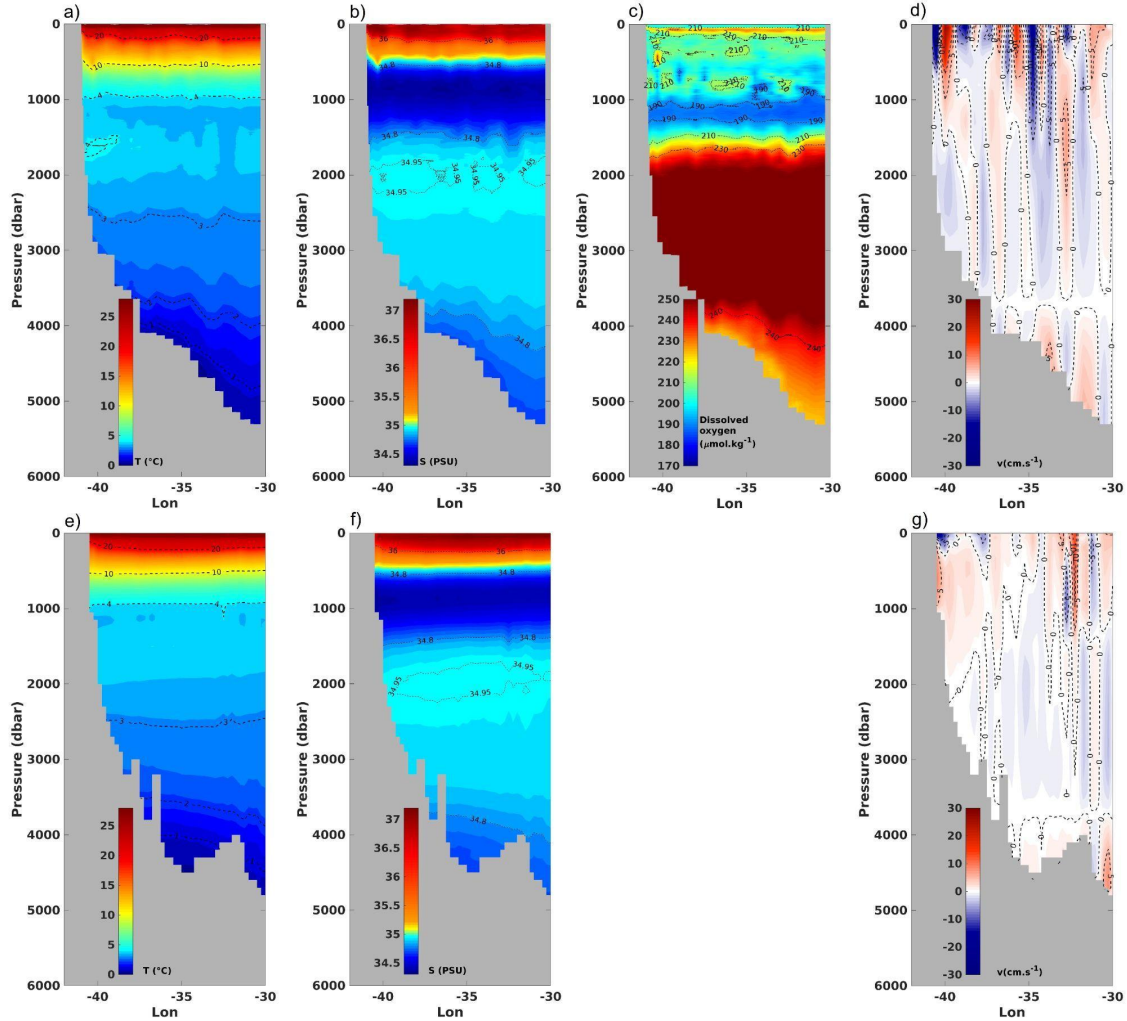


**Figure S1.** Ocean tracers and velocity section focused on Western boundary for March 2018 at 24 and 22.5°S. A-d (e-h) panels represent WOCE (AXMOC) dataset. Temperature (T), salinity (S), dissolved oxygen and velocity (v) are shown between Western boundary and 30°W.

**Text S2-S4.**

AXMOC data are compared to two synthetic observational time series from Dong et al. (2021) at 20 and 25°S and to a model reanalysis (ECCO4) at 22.5°S (Figures S2-S4). The Ekman contribution is similar among all products because consecutive versions of ECMWF products are used for Ekman contribution to AMOC transport (ERA Interim and ERA5 - Figure S2). Larger spread in geostrophic AMOC contribution is responsible for the differences in total AMOC time series among products. Dong et al. (2015) reported a

decrease in the AMOC, a decrease in the Ekman transport and an increase in Geostrophic transport toward the Equator. This pattern is also observed in this study when comparing the transects from Dong et al. (2021) at 25°S the AXMOC transect at 22.5°S, and Dong et al. (2021) at 20°S for the total AMOC (19.30±2.20 Sv, 17.21±2.72 Sv and 16.45±2.13 Sv, respectively) and from Dong et al. (2021) at 25°S, ECCO4 at 22.75°S, AXMOC transect at 22.5°S and Dong et al. (2021) at 20°S for the Ekman (-3.70±1.42 Sv, -5.01±1.38 Sv, -5.41±1.49 Sv and -6.26±1.66 Sv, respectively) transports (Figure S2 and Table 1). Overall, the meridional dependence is also observed when considering both the Ekman and the Geostrophic components. The ECCO4 product has a weaker AMOC time mean transport (14.11±2.55 Sv) than the other products (>16.45 Sv). This is because of a smaller contribution of Geostrophic transport (Figure S2 and Table 1). The total AXMOC time mean AMOC strength is 17.21±2.2.72 Sv, while in Dong et al., (2021) data the AMOC strength is 16.45±2.13 Sv and 19.30±2.20 Sv at 20 and 25°S, respectively. Therefore, the AXMOC data has higher AMOC variability than the other products. This result highlights the importance of in situ data, especially at the Western boundary, which samples the highly variable BC. Table 1 also describes the mean MHT and their variability (using the standard deviation metric as a proxy). The Ekman contribution to the MHT follows the same latitudinal dependence as the AMOC, whereas the MHT values decrease towards equator (intensification of poleward transport): -0.33±0.13 PW, -0.39±0.10 PW, -0.42±0.10 PW, -0.58±0.14 PW for Dong et al., (2021) (25°S), ECCO4 (22.75°S), AXMOC (22.5°S) and Dong et al., (2021) (20°S), respectively. The MHT Geostrophic component is 1.21±0.16 for the AXMOC product, 1.20±0.09 PW and 1.01±0.12 PW for Dong et al., (2021) at 20 and 25°S, respectively, and the weaker MHT is represented by ECCO4 reanalysis (0.87±0.10 PW). The less intense total MHT is also observed in ECCO4 data (0.48±0.16 PW), followed by Dong et al., (2021) at 20°S and 25°S (0.62±0.17 PW and 0.68±0.17 PW, respectively) and AXMOC (0.79±0.18 PW).

The monthly climatological averages of the in situ based AMOC and MHT show a multiple peak pattern, with intense transports in May and December, and a negative value in September, considering the period between 2007 and end of 2019 (Figure S3). The same pattern is observed for Dong et al., (2021) data in the period analyzed but for different peak months, with positive peaks in April and December (May and December) and a negative peak in August (October) for 20°S (25°S). For the total period analyzed in Dong et al., (2021), from 1994 to 2020, the MHT monthly climatology has a positive peak in April and a negative peak in August. The ECCO4 monthly climatological averages show a positive peak in May and two negative peaks in February and October, considering the period between 2007 and 2017. The Ekman transport contributes positively for the AMOC from December to June and negatively from July to November in every data analyzed. The Ekman component influences the total AMOC seasonality in the second semester by weakening the total transport for AXMOC and Dong et al., (2021) data. The AXMOC AMOC seasonal component presents a greater correlation to Dong et al. (2021) at 25°S than at 20°S (r= 0.80 and r=0.46, respectively).

The auxiliary data also agrees with AXMOC in the interannual signal (Figure S4). Similar to what is observed in the AXMOC dataset, most of the variability of the AMOC is explained by the geostrophic component in interannual frequencies on the synthetic

observations and ECCO4 datasets. Synthetic observations presented a significant correlation between the total and geostrophic AMOC components on the interannual signal, however, the correlation found at 25°S is similar to what it is observed for the AXMOC data (r=0.93), while the correlation at 20°S is slightly lower (r=0.65). Therefore, on both seasonal and interannual time series, the AXMOC dataset had similar correlations to the ones observed at 25°S by Dong et al., (2021) synthetic observations.
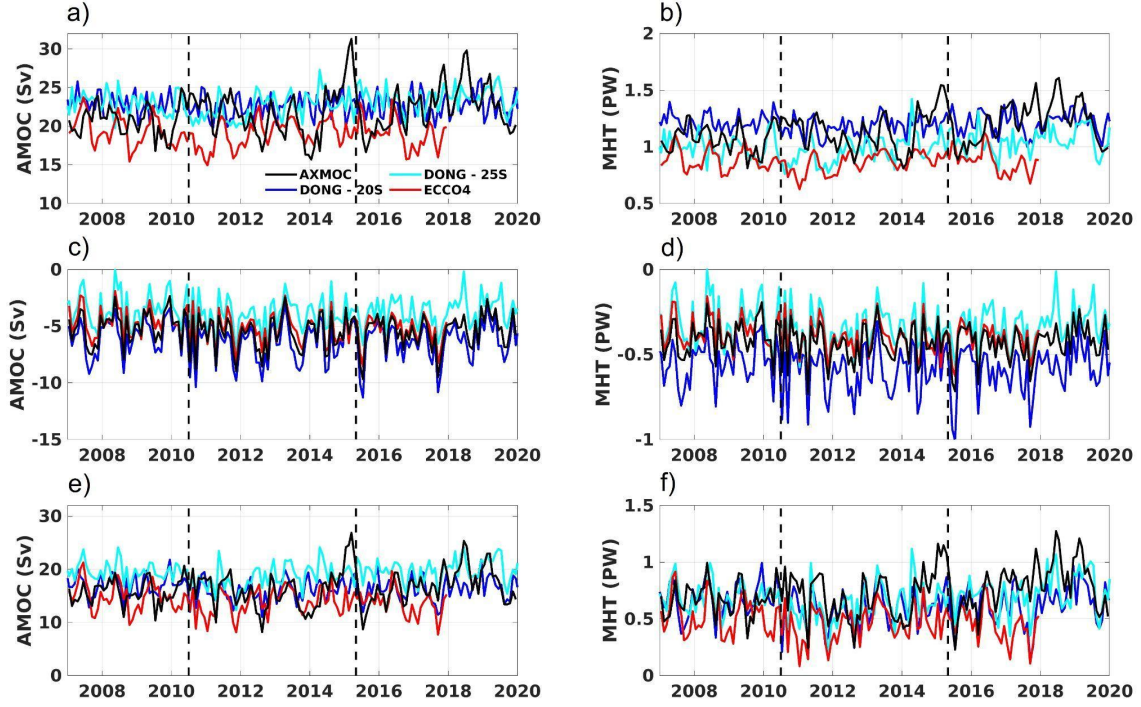


**Figure S2.** AMOC (a, c and e) and MHT (b, d and f) time series are divided into Geostrophic (a and b), Ekman (c and d) and total components (e and f). Black line represents AXMOC data. Synthetic data from Dong et al., (2021) are shown in blue (20°S) and cyan (25°S) lines. ECCO4 data is represented by the red line. Black dashed lines indicate dates of 06/2010 and 04/2015.
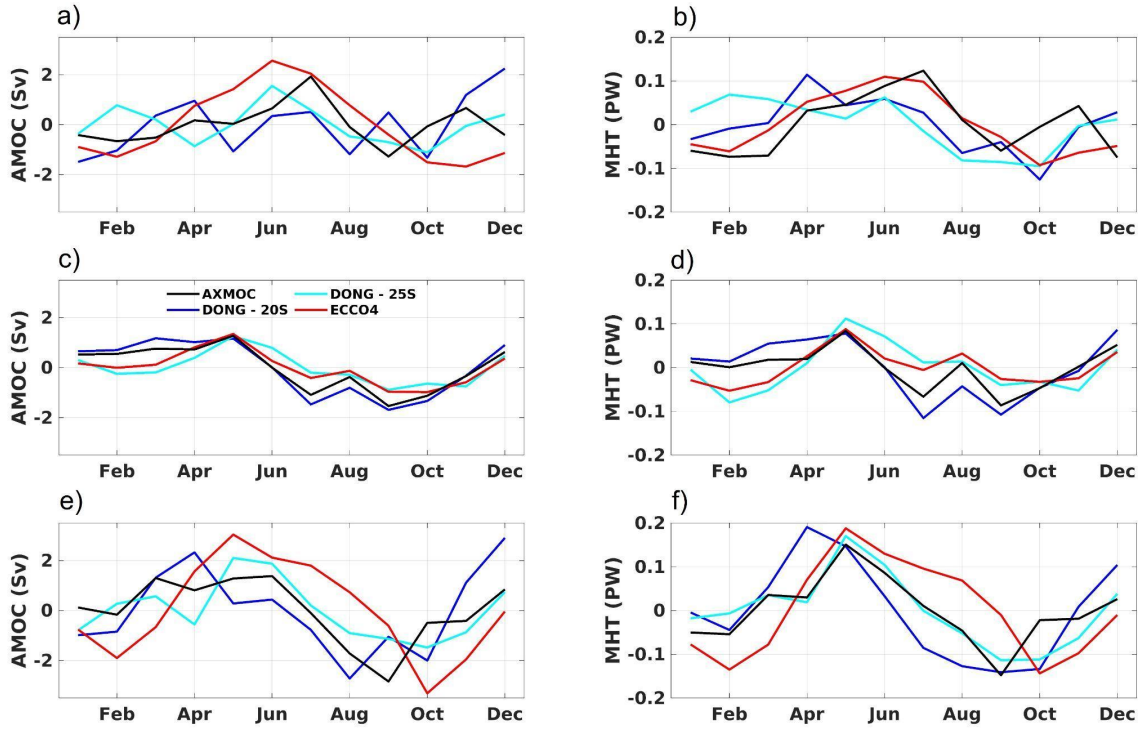
**Figure S3.** Same as Figure S2 but for the seasonal cycle. The annual mean was removed for better visualization.
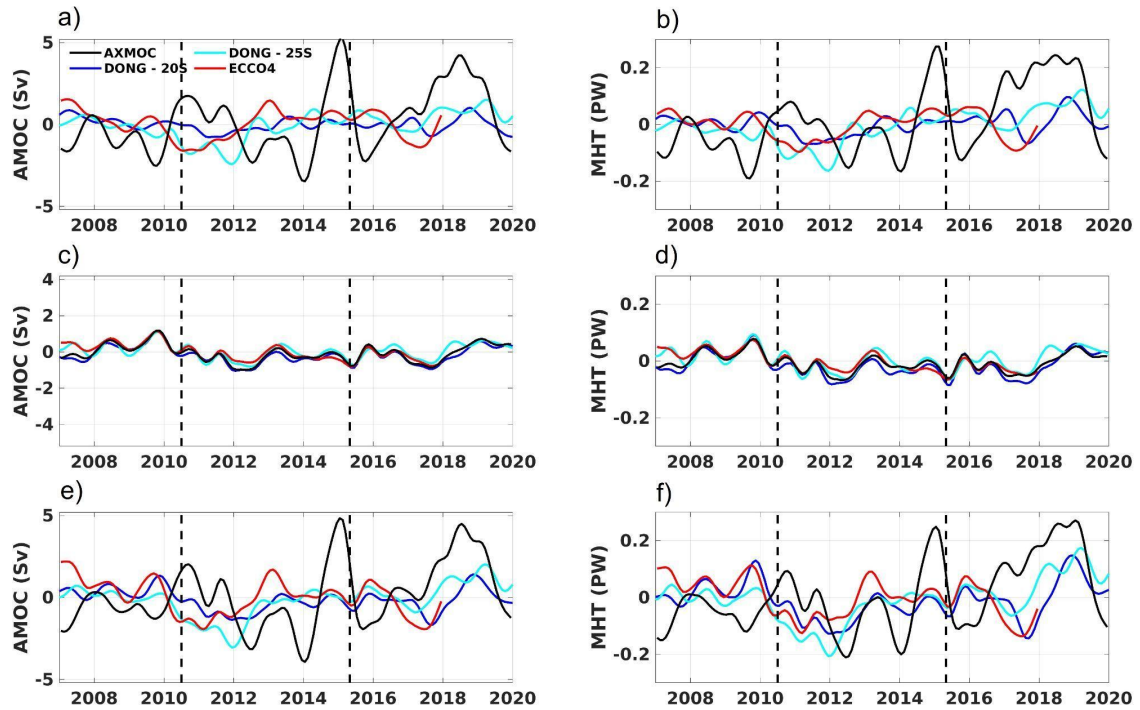


**Figure S4.** Same as Figure S2, but for the interannual component.